The electronics of the energy plane of the NEXT-White detector

V. Álvarez[a,*], V. Herrero[b], R. Esteve[b], A. Laing[a], J. Rodríguez[a], M. Querol[a], F. Monrabal[c], J. F. Toledo[b], J.J. Gómez-Cadenas[e,d,a]

[a] *Instituto de Física Corpuscular (IFIC), CSIC & Universitat de València Calle Catedrático José Beltrán, 2, 46980 Paterna, Valencia, Spain*

[b] *Instituto de Instrumentación para Imagen Molecular (I3M), Centro Mixto CSIC - Universitat Politècnica de València Camino de Vera s/n, 46022 Valencia, Spain*

[c] *Department of Physics, University of Texas at Arlington Arlington, Texas 76019, USA*

[d] *Donostia International Physics Center (DIPC) Paseo Manuel Lardizabal 4, 20018 Donostia-San Sebastian.*

[e] *IKERBASQUE, Basque Foundation for Science, 48013 Bilbao, Spain.*

Abstract

This paper describes the electronics of NEXT-White detector PMT plane, a high pressure xenon TPC with electroluminescent amplification (HPXe-EL) currently operating at the Laboratorio Subterráneo de Canfranc (LSC) in Huesca, Spain. In NEXT-White the energy of the event is measured with excellent resolution by a plane of photomultipliers (PMTs) located behind a transparent cathode. The PMTs are Hamamatsu R11410-10 chosen due to their low radioactivity and good performance. The electronics have been designed and implemented to fulfill the strict requirements both on energy resolution and radiopurity. All the components and materials have been carefully screened to assure a low radioactivity level and at the same time meet the required front-end electronics specifications such as linearity and low noise. In order to reduce low frequency noise effects and enhance detector safety a grounded cathode connection has been used for the PMTs. This implies an AC-coupled readout and baseline variations in the PMT

*Corresponding author.
Email address: vicente.alvarez@ific.uv.es (V. Álvarez)

Preprint submitted to Journal of Nuclear Instruments and Methods in Physics Research Section A May 23, 2018

signals. A detailed description of the electronics and a novel approach based on a digital baseline restoration to obtain a linear response and handle AC coupling effects is presented.

Keywords:
Calometry, Front-end electronics, Digital Baseline Restoration

1. Introduction

The NEXT program is developing the technology of high-pressure xenon gas Time Projection Chambers (TPCs) with electroluminescent amplification (HPXe-EL) for neutrinoless double beta decay searches ($Q_{\beta\beta}$) [1, 2, 3, 4, 5]. The NEXT-White[1] detector implements the second phase of the program. NEXT-White is a $\sim$ 1:2 scale detector of NEXT-100. The TPC has a length of 664.5 mm and a diameter of 522 mm a factor of two the dimensions of the NEXT-100 TPC, 100 kg HPXe-EL detector, which constitutes the third phase of the program and is foreseen to start operations in 2019. NEXT-White has been running successfully since October 2016 at Laboratorio Subterráneo de Canfranc (LSC). Its purpose is to validate the HPXe-EL technology in a large-scale radiopure detector.

This paper describes the front-end electronics of the plane of photomultipliers (PMTs) used to measure the energy of the events in NEXT-White, the so-called, *energy plane*. The organization is as follows. Section 2 summarizes the main features of the detector. Section 3 presents the front-end electronics. Conclusions are presented in section 4.

2. The NEXT-White detector

Figure 1 shows a drawing of the NEXT-White detector [6]. The main components are:

A Time Projection Chamber (TPC), that defines the detector fiducial volume. The TPC has a total length of 664.5 mm, a drift length of (530.3 ± 2.0) mm and 454 mm diameter. It contains 5 kg of xenon mass in the active volume at 15 bar. Structurally the TPC consists of: a field cage; two transparent grids, one at the cathode and one at the end of the drift region (called the gate); a quartz plate coated with a thin layer of Indium tin-oxyde

[1] Named after Prof. James White, our late mentor and friend.

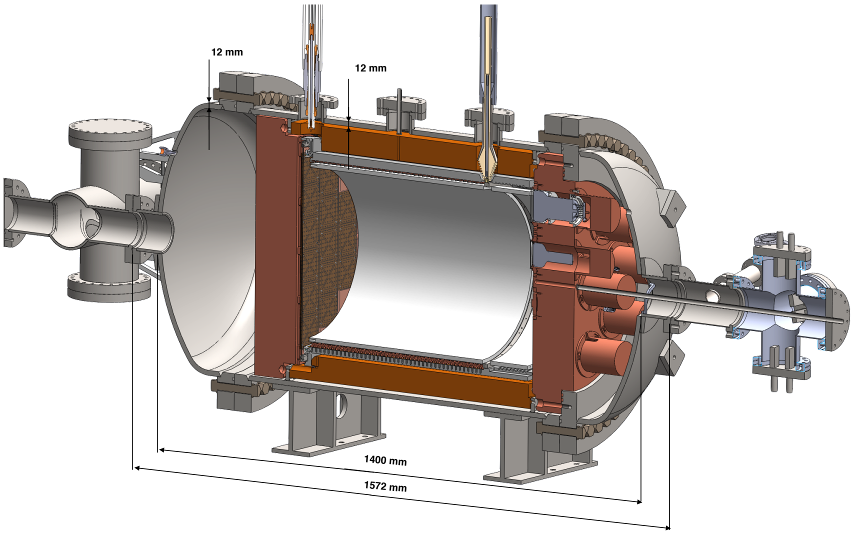

Figure 1: The NEXT-White detector

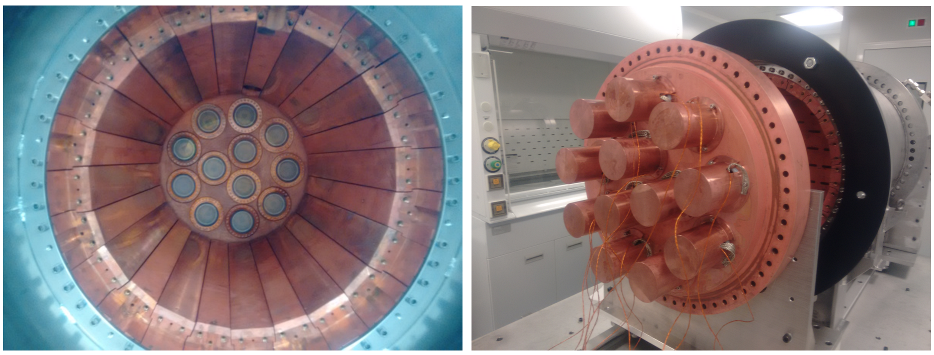

Figure 2: Left panel: the energy plane viewed from the anode, showing the sapphire windows coated with TPB; right panel: The copper hats that protect the PMTs and shield from external radiation.

(ITO), a conductor material used to properly define the anode voltage in the surface of the plate, and a thin layer of Tetraphenyl Butadiene (TPB), commonly used in noble gas detectors to shift VUV light to the visible spectrum [7]; and two high voltage feedthroughs (HVFT), which are used to set the voltages at the cathode and the gate. Functionally, the TPC includes the drift region which defines the fiducial mass of the detector, the buffer region, needed to smoothly degrade the high voltage at the cathode to ground and the electroluminescent (EL) region, where each drift electron is amplified. Each electron entering the EL region is accelerated by the higher electric field. The accelerated electrons collide with the gas atoms exciting them and producing scintillation light emmited in VUV in the case of xenon. The number of photons emitted, the optical gain n_γ, depends on the electric field in the EL region, the gas pressure and the width of the region and, in NEW, is typically set to 1000 photon electrons^{-1}.

A tracking plane, located behind the anode and equipped with 1792 SiPMs SensL series-C SiPMs distributed at a pitch of 10 mm. The spaces between SiPMs are covered by a thin (2 mm) teflon layer that increases the total anode reflectivity and enhances light collection by the PMTs.

An energy plane (figure 2) equipped with 12 Hamamatsu R11410-10 PMTs located 130 mm behind the cathode and covering 31% of its surface area. This level of coverage was chosen as a compromise between the need to collect as much light as possible for physics measurements and the need to minimize the number of sensors to reduce cost, technical complexity and radioactivity. The selected model is a 3 " PMT specially developed for low-background operation, equipped with a synthetic fused silica window and a bialkali photocatode of high quantum efficiency. The PMTs receive high voltage and have their signal extracted via kapton twisted cables connected to a feedthrough in the torispherical head of the pressure vessel. The distribution of signal and supply at each individual PMT is done by means of a Kapton circuit board (PMT base) which is covered with a copper cap and filled with epoxy. PMT bases are connected to the support plate to allow generated heat to be dissipated under vacuum conditions.

Since the Hamamatsu R11410-10 can not operate at high pressure, they are separated from the active volume by a 120 mm copper plate. The hermetically sealed PMT region is then filled with one atmosphere of N_2. The PMTs are coupled to the xenon gas volume through 12 windows, machined in the copper plate and closed with sapphire windows. The windows are coated with a resistive (and very transparent) compound Poly Ethylenedioxythiophene (PDOT) [8] in order to define a ground while at the same time avoiding sharp electric field components near the PMT windows and a thin layer of TPB.

3. Front-end electronics of the NEXT-White energy plane

One of the most distinctive features of an HPXe-EL is its excellent energy resolution, with an intrinsic limit (given by the Fano factor) of about 0.3% FWHM at the xenon $Q_{\beta\beta}$ (2.458 MeV). The NEXT prototypes [9] as well as the initial results of NEXT-White [10] have also demonstrated an energy resolution for point-like particles (Krypton X-rays) which extrapolates to 0.5% at $Q_{\beta\beta}$ (assuming naive scaling $\sigma_{Q_{\beta\beta}} \sim \sigma_{Kr}/\sqrt{E}$) and to better than ~ 0.7 % FWHM for extended tracks.

The electronics for the NEXT-White energy plane PMTs has been designed to preserve the intrinsic resolution characterizing an HPXe-EL, as well as to minimize the radioactive budget. For the latter purpose, all the components and materials have been carefully screened. A grounded cathode has been chosen in order to simplify structural design removing the need of a housing isolation. Also a remarkable reduction of low frequency noise effects has been achieved by using this connection strategy. The design has been optimized to preserve linearity over the whole dynamic range. This is a crucial feature, in particular to measure the energy of high-energy electrons which result in long tracks in the chamber (and therefore in signals as long as 100 µs). To cope with those long signals, the base circuit must provide enough charge for the PMT with negligible change in dynode-to-dynode voltage. Changes in these voltages introduce a time varying gain resulting in a nonlinear distortion mechanism and has a strong effect on PMT behavior and linearity which must be carefully controlled.

Table 1: Radioactive ^{214}Bi budget of NEXT-White PMTs and base circuits.

Component	^{214}Bi activity
PMT	0.35 mBq unit^{-1}
Base	
Capacitors 1.5 microF	72 µBq unit^{-1}
Capacitors 4.7 microF	123 µBq unit^{-1}
Finechem resistors	4.1 µBq unit^{-1}
KOA RS resistors	7.7 µBq unit^{-1}
Pin receptacles	1.1 µBq unit^{-1}
Araldite epoxy	1.4 mBq kg^{-1}
Kapton-Cu cable	46.8 mBq kg^{-1}
Kapton substrate	23 µBq unit^{-1}
Copper cap	12 µBq unit^{-1}
Total base	1.2 mBq unit^{-1}

3.1. PMT base circuit

The PMT base is a passive circuit involving 19 resistors of different electrical resistance, 7 capacitors (3 having a capacitance of 1.5 µF and 4 with 4.7 µF) and 18 pin receptacles soldered on a kapton circuit board and covered with thermal epoxy [11] (figure 3 top panel and bottom right) to

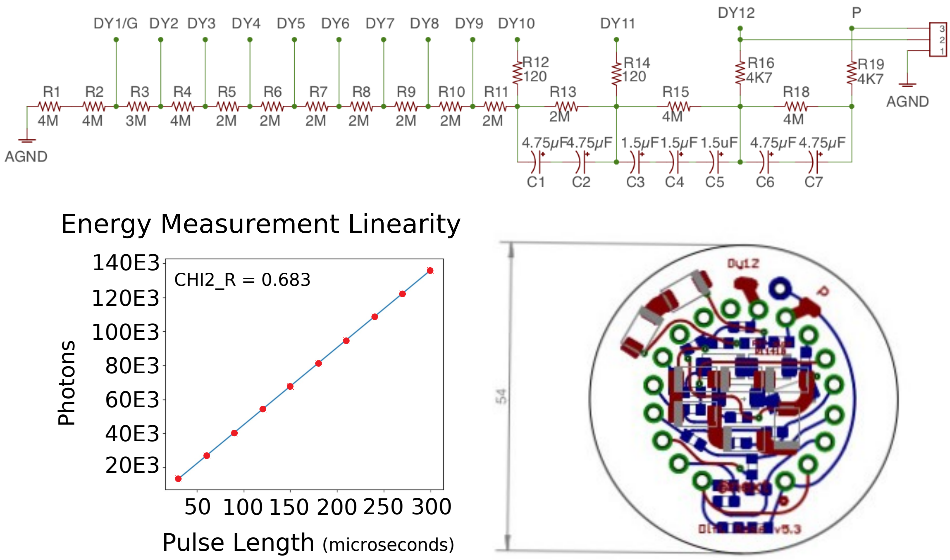

Figure 3: Top: NEXT-White PMT base circuit; bottom-left: Fit to the response of the PMT plus base, showing excellent linearity; bottom right: base layout.

avoid dielectric breakdown in moderate vacuum or in a N2 atmosphere, and to improve thermal contact with the copper hat. It has been designed to optimize the tradeoff between the conflicting targets of preserving the signal linearity (figure 3 bottom left) and keeping the radioactive budget to a minimum. The difficulty to achieve both goals simultaneously resides in the fact that the stringent requirements to keep a linear response —the design demands that the maximum expected signal introduces a voltage drop no larger than 0.1% of the voltage between dynodes— requires the use of capacitors to hold the charge in the latest amplification stages, where the gain is very large. The linearity fit gives a 0.38% for an input of 140×10^3 photoelectrons which exceeds the maximum charge expected per time bin in the PMTs.

The tradeoff is the radioactivity introduced by the base, which is four times larger than that of the PMT itself, as shown, for ^{214}Bi activity in table 1 (see [12] for a thorough discussion). Notice, however, that the radioactivity injected in NEXT-White by the base is partially shielded by the copper shield, and contributes roughly the same to the final background count as the PMTs.

The resistor chain value ratios have been recommended by the PMT manufacturer and the final value of the resistors have been adjusted to reduce power dissipation. A power of 40 mW results in a stable temperature of 30 °C for a 21 °C ambient temperature which introduces no disturbances in the rest of the detector. The number of capacitors —which are the most radioactive elements in the base– have been kept to a bare minimum. They are only introduced in the last three amplification stages where the amount of charge to be delivered by the PMT is higher and needs to be held with the help of capacitors.

3.2. Grounded Cathode PMT connection and its consequences

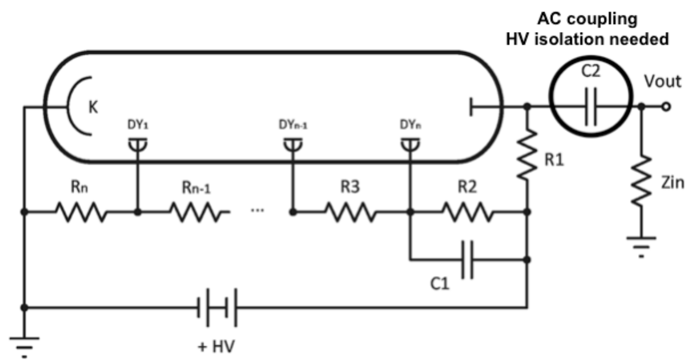

Figure 4: Grounded Cathode PMT connection scheme.

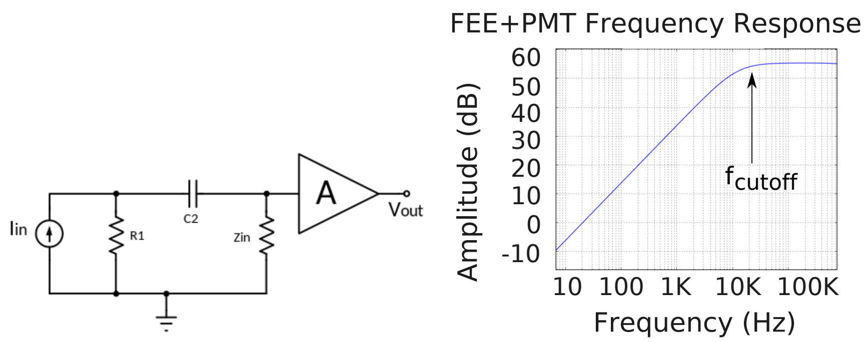

Figure 5: Grounded Cathode Equivalent Circuit and Frequency response.

In NEXT-White the PMTs' photocathodes (and thus their bodies) are connected to ground, while the anode is set at the operating voltage of the PMT (1.23 kV). This solution simplifies the detector mechanics and enhances safety (the alternative, with the cathode and the PMT body at high voltage would have required the insulation of each PMT from ground). In exchange, the anode output needs to be AC coupled through an isolation capacitor, as shown in figure 4, since the anode output DC voltage equals the high voltage being applied to the PMT.

An AC coupling scheme creates, to first order, a high pass filter (HPF). Figure 5 (left panel) shows the electrical equivalent circuit of the connection scheme, modeling the PMT as a simple current source. The Laplace transfer function of the filter (right panel of figure 5) is defined by equation 1:

$$\frac{v_O}{i_I} = A\frac{Z_{in}R_1}{Z_{in}+R_1}\frac{(R_1+Z_{in})C_2s}{1+(R_1+Z_{in})C_2s} \tag{1}$$

where R_1 is the high value resistor which mainly defines the filter along with the decoupling capacitor C_2s. The filter blocks the DC component and attenuates frequency components below the cutoff frequency f_{cutoff} (see figure 5, right), defined as:

$$f_{cutoff} = \frac{1}{(R_1+Z_{in})C_2 \cdot 2\pi} \tag{2}$$

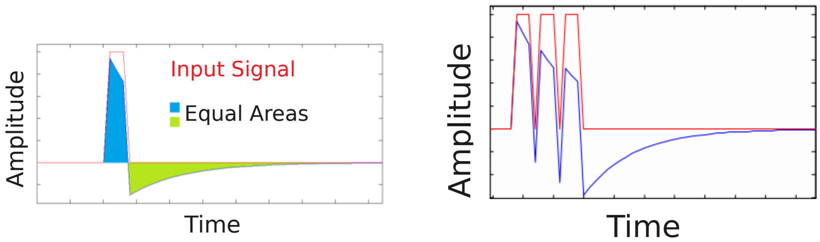

Figure 6: The effect of a HPF in a square pulse (top panel) and in a train of square pulses (bottom panel).

The effect of the HPF on a square pulse and on a train of square pulses is shown in Figure 6. The output pulse after the filter is the derivative of the input pulse, and is characterized by a null total area. Since the energy is proportional to the area of the input pulse, it follows that a deconvolution (or baseline restoration) algorithm must be applied to the output pulse in order to recover the input pulse area and thus measure the energy. Also, since the intrinsic energy resolution in NEXT-White is very good the error introduced by the deconvolution algorithm must be, at most, a fraction per mil.

Indeed, the simple model of the PMTs as an ideal current source is insufficient given the accuracy required and must be refined in a number of ways. For example, the effect of the charge exchange between the capacitors of the PMT base and the coupling capacitor, must be included in the model (figure 7). The resulting filter, shown in figure 8 is then more complicated

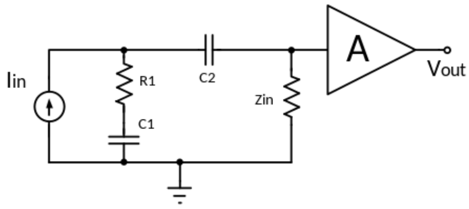

Figure 7: A more sophisticated model of the FEE + PMT base.

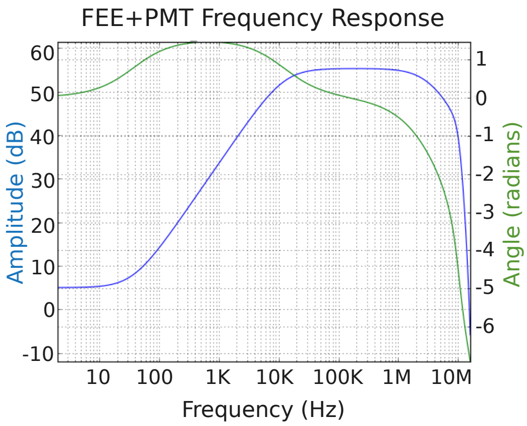

Figure 8: FEE Full Frequency Response.

than a simple HPF, but can still be accurately described as a pole/zero combination obtained from the equivalent circuit shown in figure 7. The filter follows the equation:

$$\frac{v_O}{i_I} = \frac{Z_{in}}{(1+\frac{C_1}{C_2})} \frac{1 + R_1 C_1 s}{1 + \frac{(R_1+Z_{in})C_1}{(1+\frac{C1}{C2})} s} \tag{3}$$

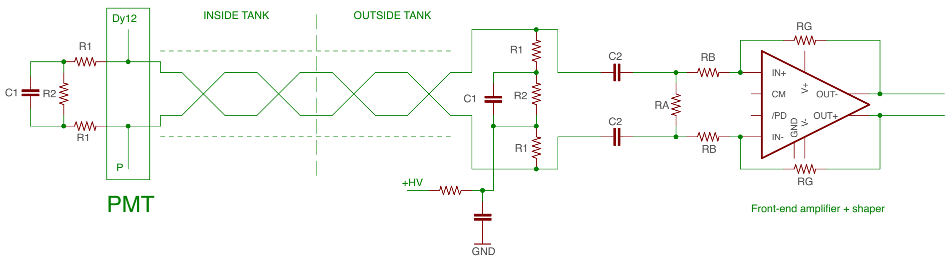

Figure 9: FEE Scheme

The active components in the FEE have been chosen to minimize noise. The bandwidth of the FEE (3MHz) makes it work as a shaping filter, stretching the time length of the single photo-electron response that was provided as a specification by the detector calibration team. A simplified version of the FEE is shown in fig. 9. A pseudo-differential transmission has been chosen in order to reduce coupled noise which is expected to be high, since the distance between the FEE rack and the NEXT-White pressure vessel is about 12 meters. The AC coupled enables the use of the same cable for both supply voltage and signal extraction

3.3. Noise Measurements

In order to check the specifications of the design, noise measurements have been carried out in the laboratory and at the LSC NEXT installation. The results are shown in the table 2.

The worst case total noise is 0.8 LSB, which is within specifications. The theoretically computed noise of the FEE was 0.35 LSB without power supply contribution. The indirectly measured FEE noise contribution is 0.36 LSB, very close to specifications. The remaining noise can be attributed to the DAQ system.

Table 2: Noise Measurements (in LSB_{rms})

		Laboratory	LSC NEXT
Direct Measurement	DAQ	0.64	0.66
	FEE + DAQ	0.75	0.75
	FE + DAQ + PMT	0.76	0.8
Indirect Measurement	FE	0.39	0.36
	PMT	0.12	0.28

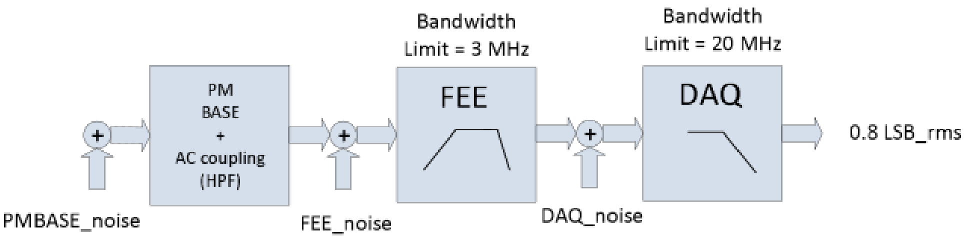

Figure 10: Noise generation scheme.

3.4. Front End Electronics model for simulation

The FEE model incorporates the filter described by equation 3 plus a fourth order low pass filter, due to the required shaping (see figure 8). The model response is consistent with detailed SPICE simulations of the implemented FEE.

Noise is introduced in the model following the behavior of the real system, that is, taking into account the filtering effect of every part. For instance, the input equivalent noise of the FEE has been increased to show its true effect given the 3 MHz bandwidth. The noise equivalent model of the FEE is shown in figure 10 and described by equations 4.

$$\begin{aligned}
GAIN &= FEE_{GAIN}.DAQ_{GAIN} \\
vo^2_{TOTAL_{noise}} &= v^2_{DAQnoise}(out) + v^2_{FEE+PMBnoise}(out) \\
vo^2_{TOTAL_{noise}} &= \int_0^{BW=3MHz} v^2_{FEE+PMBnoise}.|GAIN.H(jw)|^2 \\
&+ \int_0^{BW=20MHz} v^2_{DAQnoise}.|DAQ_{GAIN}.H(jw)|^2 \\
vo_{TOTAL_{noise(rms)}} &= \sqrt{vo^2_{TOTAL_{noise}}} = 0.76LSB_{rms} \qquad (4)
\end{aligned}$$

The baseline restoration (BLR) algorithm is based on the implementation of the inverse function of a HPF. The impulse response of this inverse function has a structure composed of a delta in the origin plus a step function whose amplitude equals the value of $\frac{1}{\tau}$ where τ is $(R_1 + Z_{in}).C$ (equation 5). This means that the convolution operation can be carried out using just an accumulator and a multiplier instead of a more complex FIR filter.

$$\begin{aligned} HPF^{-1}(s) &= 1 + \tfrac{1}{\tau.s} \\ HPF^{-1}(t) &= \delta(t) + \tfrac{1}{\tau}\int_0^t dt \end{aligned} \tag{5}$$

(a) HPF Inverse impulse response (b) MAC implementation

Figure 11: Inverse HPF Implementation.

A nice feature of this algorithm is that it can be activated when a pulse is detected and then switched off when the pulse ends. This means that a sizable amount of low frequency noise filtered by the AC coupling capacitor will not be reintroduced in the system, since it is slower than the pulse length. On the other hand, the low frequency zero introduced by the PMT base interaction adds a low amount of DC to the theoretically AC coupled output signal of the FEE. In order to cancel this effect a high pass filter with a cutoff frequency equal to the frequency of this zero is introduced previous to the BLR algorithm. This completely cancels the DC effect so that the reconstructed signal shows no baseline shift at the end.

Any algorithm based on a simple accumulator is sensitive to noise. In particular, the residual low frequency components of the noise leave a small residue in the accumulator. Due to finite sampling of the signals, this residue does not always cancel. For instance in a burst of short signals (photoelectrons) the residue tends to be positive because the pulses have a

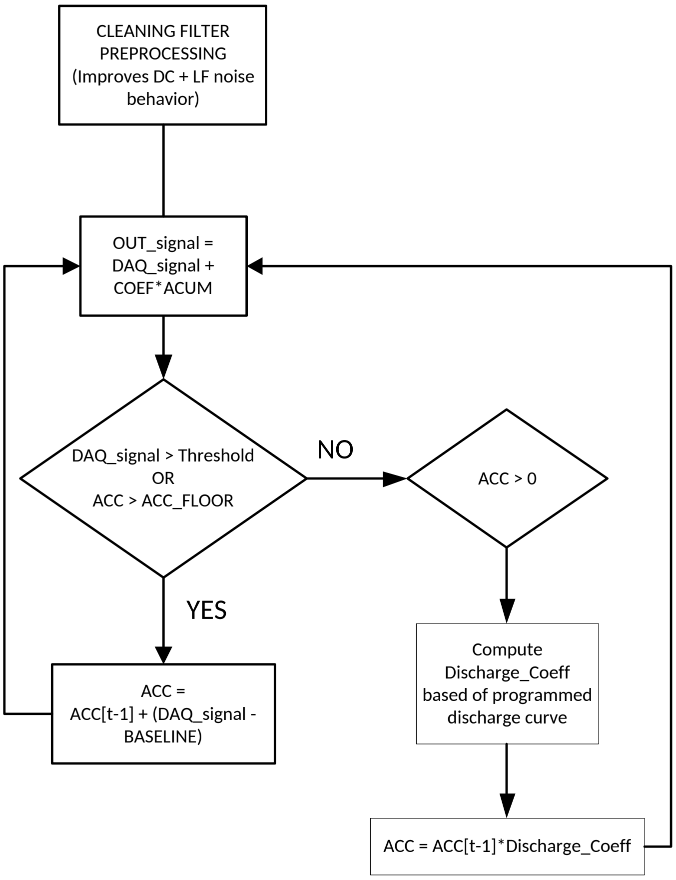

Figure 12: Accumulator based BLR.

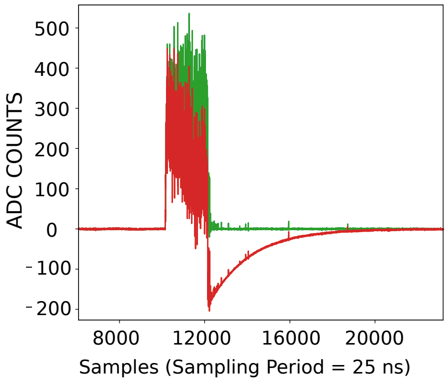

(a) Red - Real input signal; Green - FEE output signal

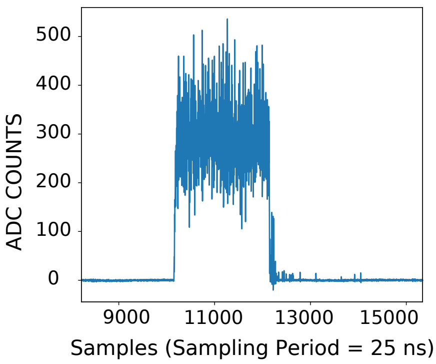

(b) Digital baseline reconstruction applied

Figure 13: Signal from simulation of 50 μs pulse. 25865 pe. Noise 0.74 LSB

higher positive lobe. As a consequence the accumulator keeps increasing, introducing a baseline shift in the output signal.

The BLR algorithm developed for the NEXT-White energy plane controls the rise of the accumulator using a mechanism to smoothly deplete the residue remaining in the accumulator after a pulse reconstruction. The algorithm flowchart is shown in fig. 12. Notice that in this algorithm the reconstruction process is started independently from the beginning of the pulse, and can in principle be active continuously. The control relies on the accumulator operations that can be *Update* or *Discharge*. When the raw signal (coming from the DAQ) rises above a threshold or the accumulator value is above another threshold (which is the condition for an active pulse) the accumulator is updated as in the original algorithm. However when none of those conditions are met, which means that there is no active signal pulse, the accumulator is forced to a controlled discharge state. This discharge operation is carried out following a smooth curve so that the reconstructed signal shows no jumps or discontinuities. As an example of the action of the BLR algorithm, figure 13 shows the output signal of a PMT (showing the characteristic negative swing introduced by the filter) and the corrected signal after the BLR algorithm.

The estimated residual in the energy correction has been computed applying the deconvolution to Monte Carlo signals generated using the detailed simulation described above and the effect has been quantified to be smaller than 0.3 % FWHM for long signals (corresponding to large energies), and thus introducing an effect smaller than the resolution due to the Fano factor.

3.6. Deconvolution of the PMT raw waveforms in ^{83m}Kr *calibration data*

NEXT-White has been operating at the LSC since October 2016. The detector has been calibrated with data taken with a ^{83}Rb source connected to its gas system [6]. The exotic rubidium isotope decays to ^{83m}Kr via electron capture with a lifetime of 86.2 days. The krypton then decays to the ground state by emitting two electrons at 95% BR. A Kr decay results in an energy deposit of low enough energy to be considered point-like.

The raw data produced by the energy plane are PMT waveforms, sampled each 25 ns. The HPF associated to the grounded cathode scheme introduces a negative swing in the PMT waveforms. The first step in the data processing is to apply the BLR algorithm described above to the arbitrary-baseline, uncalibrated raw-waveforms (RWFs), to produce positive-only, zero-baseline, calibrated waveforms (CWFs). Figure 14 shows the RWFs corresponding to the PMTs of the energy plane, while Figure

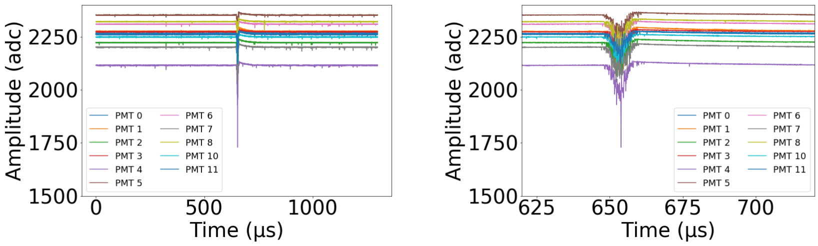

Figure 14: ^{83m}Kr raw waveforms for the individual PMTs, showing the negative swing introduced by the PMTs front-end electronics. The left panel shows the RWF in the full data acquisition window, while the right panel shows a zoom on the EL-amplified signal (S_2) on which event read-out was triggered.

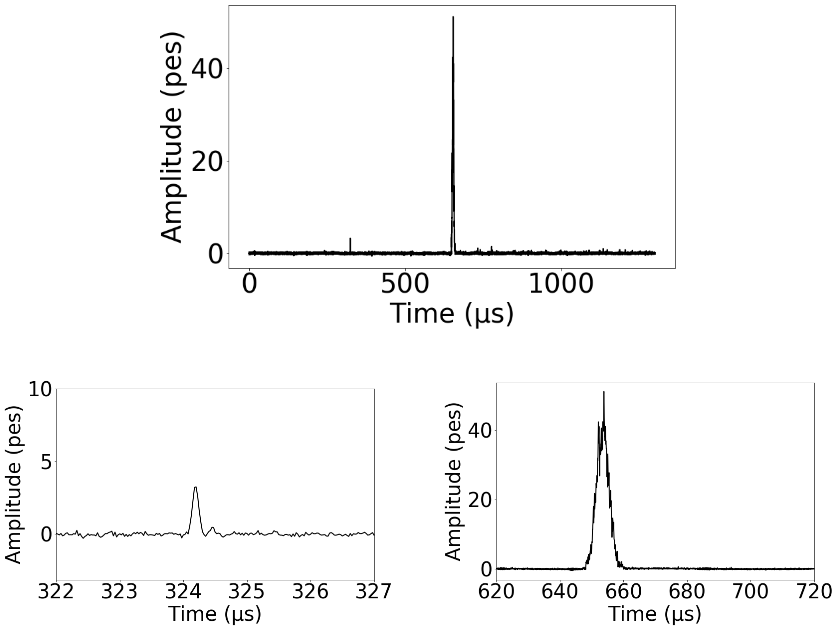

Figure 15: ^{83m}Kr corrected waveforms for the sum of the PMTs. The top panel shows the corrected waveform in the full data acquisition window, while the bottom panels show zooms of the primary scintillation signal (S_1) –left panel– and EL-amplified signal (S_2) –right panel– waveforms.

15 shows the CWF waveform corresponding to the PMT sum. The event was triggered by the EL-amplified signal (S_2) which appears centered in the data acquisition window (DAQW). The primary scintillation signal (S_1) signal appears at the beginning of the DAQW.

The deconvolution procedure permits full recovery of the energy of the waveforms. Indeed, the measured energy resolution for ^{83m}Kr point-like energy deposits in NEXT-White at 7.2 bar is $(4.55 \pm 0.04)\,\%$ (which extrapolates $1/\sqrt{E}$ to $(0.592 \pm 0.005)\,\%$) in the full chamber and $(3.88 \pm 0.05)\,\%$ ($(0.504 \pm 0.006)\,\%$) in a fiducial region ($r < 150\,\text{mm}, z < 150\,\text{mm}$) chosen to minimize the effect of lower solid angle coverage and large lifetime corrections [10]. The energy resolution we obtain is remarkably close to the intrinsic value in an HPXe-EL for these conditions and shows that the BLR algorithm does not introduce unwanted residual effects in the energy resolution.

4. Conclusion

A major challenge in the design and implementation of the front-end electronics for the NEXT-White detector's energy plane is to strike the best compromise between the conflicting requirements of radiopurity and performance (linearity, high-gain, etc.) needed for high-resolution measurement of the energy. In this paper, a solution, based on the choice of radio-pure components (Kapton circuits for the PMT bases and low-radioactivity resistors and capacitors), and implementing a grounded cathode PMT connection, has been presented, together with a detailed description of the BLR algorithm which allows a high-precision measurement of the energy.

Acknowledgments

We acknowledge support from the following agencies and institutions: the European Research Council (ERC) under the Advanced Grant 339787-NEXT; the Ministerio de Economía y Competitividad of Spain under grants FIS2014-53371-C04, the Severo Ochoa Program SEV-2014-0398 and the María de Maetzu Program MDM-2016-0692; the GVA of Spain under grants PROMETEO/2016/120 and SEJI/2017/011; the Portuguese FCT and FEDER through the program COMPETE, projects PTDC/FIS-NUC/2525/2014 and UID/FIS/04559/2013; the U.S. Department of Energy under contracts number DE-AC02-07CH11359 (Fermi National Accelerator Laboratory), DE-FG02-13ER42020 (Texas A&M) and de-sc0017721 (University of Texas at Arlington); and the University of Texas at Arlington. We acknowledge partial support from the European Union Horizon 2020 research and innovation programme under the Marie Sklodowska-Curie grant agreements No. 690575 and 674896. We also warmly acknowledge the Laboratorio Nazionale di Gran Sasso (LNGS) and the Dark Side collaboration for their help with TPB coating of various parts of the NEXT-White TPC. Finally, we are grateful to the Laboratorio Subterráneo de Canfranc for hosting and supporting the NEXT experiment.

References

References

[1] David Nygren. High-pressure xenon gas electroluminescent TPC for $0-\nu$ $\beta\beta$-decay search. *Nucl.Instrum.Meth.*, A603:337–348, 2009.

[2] V. Álvarez et al. The NEXT-100 experiment for neutrinoless double beta decay searches (Conceptual Design Report). 2011.

[3] V. Álvarez et al. NEXT-100 Technical Design Report (TDR): Executive Summary. *JINST*, 7:T06001, 2012.

[4] J. J. Gomez-Cadenas et al. Present status and future perspectives of the NEXT experiment. *Adv. High Energy Phys.*, 2014:907067, 2014.

[5] J. Martín-Albo et al. Sensitivity of NEXT-100 to Neutrinoless Double Beta Decay. *JHEP*, 05:159, 2016.

[6] F. Monrabal et al. The Next White (NEW) detector. 2018.

[7] V. M. Gehman, S. R. Seibert, K. Rielage, A. Hime, Y. Sun, et al. Fluorescence Efficiency and Visible Re-emission Spectrum of Tetraphenyl Butadiene Films at Extreme Ultraviolet Wavelengths. *Nucl. Instrum. Meth.*, A654:116–121, 2011.

[8] Sigma-aldrich. `http://www.sigmaaldrich.com/catalog/product/aldrich/483095?lang=es&region=ES`.

[9] V. Álvarez et al. Near-Intrinsic Energy Resolution for 30 to 662 keV Gamma Rays in a High Pressure Xenon Electroluminescent TPC. *Nucl. Instrum. Meth.*, A708:101–114, 2012.

[10] G. Martínez-Lema et al. Calibration of the NEXT-White detector using ^{83m}Kr decays. 2018.

[11] Araldite 2011. expy adhesive in two components.

[12] S. Cebrián et al. Radiopurity assessment of the energy readout for the NEXT double beta decay experiment. *JINST*, 12(08):T08003, 2017.